2002-01

Heat Flux Gage Studies of Compressible Dynamic Stall

Chandrasekhara, M.S.

40th AIAA Aerospace Sciences Meeting and Exhibit January 14-17, 2002 / Reno, NV
http://hdl.handle.net/10945/50222

AIAA 2002-0291
Heat Flux Gage Studies of Compressible Dynamic Stall

M.S.Chandrasekhara
Navy-NASA Joint Institute of Aeronautics
Department of Aeronautics and Astronautics
Naval Postgraduate School
Monterey, CA 93943
and
M.C.Wilder
NASA Ames Research Center, M.S. 230-2
Moffett Field, CA 94035

40th AIAA Aerospace Sciences Meeting and Exhibit
January 14-17, 2002 / Reno, NV

Heat Flux Gage Studies of Compressible Dynamic Stall

M.S. Chandrasekhara[1]
Navy-NASA Joint Institute of Aeronautics
Department of Aeronautics and Astronautics
Naval Postgraduate School, Monterey, CA 93943

and

M.C. Wilder[2]
NASA Ames Research Center, M.S. 230-2
Moffett Field, CA 94035-1000

Abstract

Compressible dynamic stall was studied using 148 closely spaced heat flux gages distributed over the surface of an oscillating, 6-inch chord NACA 0012 airfoil. The study has revealed the various surface flow features of compressible dynamic stall and their changes under different flow conditions. It has also provided a description of the events that are precursors to dynamic stall onset. The imprint of a leading edge shock has been recorded for the first time in the surface flow signature. The data indicate that extremely large gradients develop prior to onset of dynamic stall, pointing to a singular event that drives the flow into the stalled state.

1. Introduction

A fundamental understanding of dynamic stall onset is important to both rotary and fixed wing aerodynamicists. Dynamic stall refers to the stall process of an airfoil executing an unsteady maneuver; e.g., sinusoidal pitch oscillations. During this maneuver the airfoil can reach angles of attack exceeding the static stall angle, and generate lift in excess of the maximum static lift. The process, however, culminates in the formation of a dynamic stall vortex, which propagates along the chord of the airfoil producing large variations in the pitching moment. These pitching moment variations associated with the dynamic stall vortex can have destructive effects on aircraft components, such as helicopter rotor blades. As a consequence, the benefit of dynamic stall, the large dynamic lift, has remained unexploited. A thorough understanding of the mechanism of dynamic stall vortex formation is necessary for developing a practical control system.

It has been shown in Ref. 1 that in the compressible regime, dynamic stall onset can occur due to a variety of causes involving small changes in the flow conditions. A measurement technique is needed that is sensitive enough to resolve the very sharp, dynamically changing flow gradients, at the leading edge boundary layer scale (≈ 250 μm) where these effects originate. It is clear that particle based optical techniques are not satisfactory for surface measurements due to incidental problems (glare, reflection and spatial resolution). In addition, they suffer from particle lag effects, which are amplified near the wall region due to the very large flow gradients. A case in point is the back side of a compressible dynamic stall vortex, where accelerations as large as 50g could be encountered. Optical techniques based on molecular properties such as density provide meaningful results, but are predominately spanwise averaged and are quite complicated. The surface flow details still cannot be captured using these techniques. Thus, it was decided to use very thin hot-film gages for sensing the surface flow. Although there is no known calibration method available for the measurement of skin friction in adverse pressure gradient driven unsteady flows, the variation of surface heat flux, throughout the oscillation cycle and at various chordwise locations, provides valuable qualitative data that can be appropriately interpreted. The global flow in this study has already been fully documented using Point Diffraction Interferometry (PDI) and the results will be used to verify the heat flux gage measurements.

Oscillating airfoil flows have been studied in the past using multiple heat flux gages (Kiedaisch & Acharya,[2] Lee & Basu,[3] Schreck et al[4, 5]) and the fundamentals involved in interpreting the heat flux gage data in steady flow have been described by Nakayama et al[6] and Stack et al[7]. The latter group pioneered the use of this technique and the fabrication of the sensors. All these studies have focused on low-speed flows. They have also been only qualitative since calibration to determine the skin friction is a challenge as mentioned above. Despite this limitation, analyzing the heat flux traces can generate significant physical insight into the flow. In all these studies, even though many sensors were used, the distribution of the sensors over the surface can still be deemed sparse. They were also limited to certain regions of the flow. In the previous studies of dynamic stall flow, the heat flux gages covered only the leading few percent of chord.

This study primarily considers unsteady compressible flow, and compressible dynamic stall in particular, and has documented the various underlying flow events. A very large number of sensors were used, covering the entire

---

[1] Research Professor and Associate Director, **Mailing Address:** NASA Ames Research Center, M.S. 260-1, Moffett Field, CA 94035-1000, Assoc. Fellow,

[2] Research Scientist, Member AIAA

upper surface and some of the lower surface, as described in the next section.

2. Description of the Experiment

148 closely spaced hot-film gages were distributed over the surface of an oscillating, 6-inch chord NACA 0012 airfoil. The leading edge from x/c = 0.1 on the lower surface to x/c = 0.25 on the upper surface was covered with sensors at a pitch of 40 gages/inch. Sets of 4 gages (with the same pitch) were mounted over the rest of the upper surface at every 5% chord. The sensors were fabricated and installed on the airfoil by NASA Langley Research Center. All sensors were operated at an overheat ratio of 1.5 at Mach numbers ranging from 0.2 – 0.45 and at reduced frequencies from 0 - 0.1. The airfoil was mounted between the sidewalls of the NASA Ames Research Center FML Compressible Dynamic Stall Facility and oscillated at $\alpha = 10^{O} - 10^{O}\sin\omega t$. The gages were connected to a bank of TSI Model 1750/1755 anemometers. Analog data from 16 hot-film gages at a time were simultaneously sampled along with the digital data of the airfoil angle-of-attack encoder using Microstar Laboratories, Inc. ADC and digital I/O boards. Sampling rates between 10-40KHz were used, for a total of 40-80K samples/channel with the airfoil oscillating at frequencies of up to 22 Hz. These large sample sets were used for ensemble averaging by binning over one encoder count (< 1 deg phase angle), which corresponds to an angle of attack of 0.08 deg or less. For all cases, an adequate number of samples (40-100) were available in each bin. The data were analyzed primarily using the ensemble averaged mean values of the hot film output voltages. In the data that are presented, the deviations from the cycle mean value at each phase angle are plotted. Since there is no calibration method available for unsteady flows, a comparison of this quantity will provide an estimate of the local ensemble averaged surface shear stress on an arbitrary scale.

In addition, comparisons with interferograms obtained in earlier research on this problem will be made where needed to confirm the various flow features that were observed in this study. This is particularly important since without a direct calibration, the only features present in the signal are either a rise or fall in the heat flux values. The meaning is clear in some instances, such as transition onset, but it needs to be studied in the context of the local flow for each condition to better establish the flow physics.

Experimental Conditions

The experiments were conducted for the following conditions.

Mach Number, M:	0.2 – 0.45
Reduced Frequency, $k = \pi fc/U_\infty$:	0 – 0.1 for M = 0.2 & 0.3, and 0 – 0.05 for M = 0.4 & 0.45
Angle of Attack, α:	$10^\circ - 10^\circ \sin\omega t$
Reynolds Number, Re:	$0.7\times10^6 - 1.6\times10^6$

3. Results and Discussion

A. Interpretation of Heat Flux Gage Output Traces

Interpretation of these data is difficult since the gages are not calibrated, and since zero surface shear stress does not represent a separated flow condition in unsteady flows. However, physical insight into some details aids in this effort. For example, a gradual thickening of the boundary layer with increasing angle of attack causes the skin friction to decrease and hence the gage output decreases. Laminar to turbulent transition causes the familiar abrupt increase in the sensor output. A laminar separation bubble is usually seen as a rapid drop in the sensor output that follows a mild reduction in output while the laminar boundary layer thickens with increasing angle of attack. Passage of the dynamic stall vortex over the airfoil upper surface leaves a trace that appears as a gradually elevated output rising towards the airfoil trailing edge as the angle of attack is increased, whereas flow reattachment shows the opposite behavior. Transition front movement appears as an increase in the output voltage, progressing towards the leading when the angle of attack is increased, whereas relaminarization manifests itself by an opposite behavior. Furthermore, in addition to these physical insights, we have generated a significant amount of global, quantitative, flow-field visualization information in our past studies of compressible dynamic stall upon which we may rely when interpreting the heat flux gage data. With this background, the results of the study are discussed below.

B. Flow Details at M = 0.3

Figure 1 shows three point diffraction interferometry (PDI) images for M = 0.3, k = 0.05, which are instantaneous quantitative flow documentations at α = 6, 8, and 13.5deg. The fringes seen in the image are constant density contours. The important flow features are indicated in the figure for future reference. Figure 2 presents the ensemble averaged gage outputs (with the cycle mean subtracted) for several angles of attack at M = 0.3, k = 0.05. At low angles, the flow is laminar over much of the upper surface (see discussion on transition below) and the traces for α = 4 and α = 5 deg confirm that the shear stress is low over the range of x/c shown (these become turbulent further downstream). For α = 6 deg, there is an abrupt rise seen at x/c = 0.08, which corresponds to boundary layer transition. At slightly higher angles, a laminar separation bubble forms, (see also Fig. 1b). When this occurs, the heat flux at x/c ≈ 0.02 drops rapidly, as can be seen for $\alpha \approx 7$ deg, and the bubble is still present at α = 12.5 deg. It is interesting to see that significant variations in the heat flux are present within the bubble region (see indicated region in Fig. 2). Over the sensors near the leading edge the heat flux keeps falling, indicating that the flow reversal is still ongoing at angles of attack higher than the bubble formation angle. These data clearly show the onset location of the bubble at x/c ≈ 0.018 – 0.02. The end of the bubble appears to be at x/c ≈ 0.08, just ahead of the location where transition was seen for the lower angle of attack of 6 deg. This can be inferred from the fact that the shear stress variations nearly coincide for $\alpha > 7$ deg here. Inside the bubble, dramatic variations occur

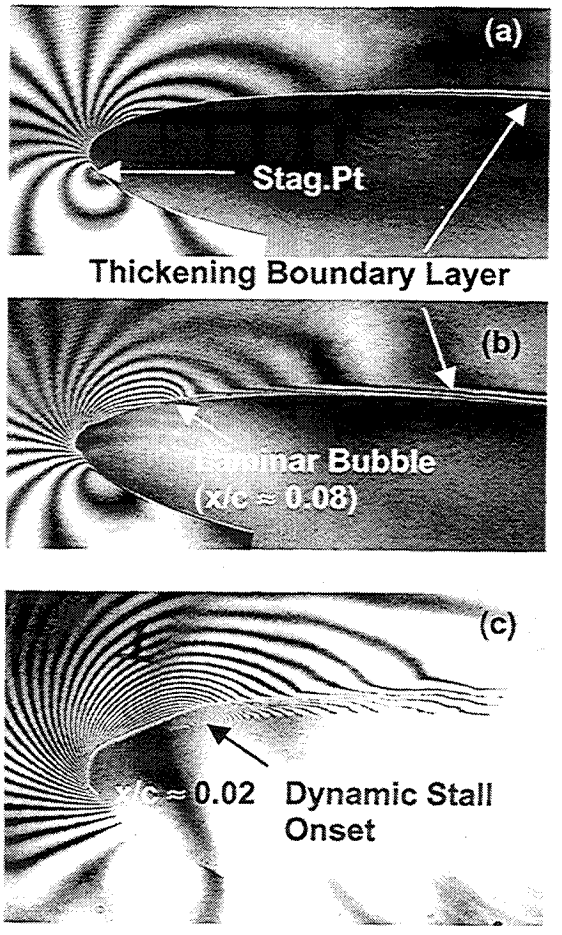

Fig. 1. PDI Images of M= 0.3, k = 0.05
Flow, (a) $\alpha = 6^{o}$, (b) $\alpha = 8^{o}$, (c) $\alpha = 13.5^{o}$

in the surface shear stress. The conventional picture of the bubble containing a low energy recirculating fluid is supported by the very low shear stress values here. Towards the end where the bubble closes, there is an increase in the shear stress as the separated shear layer becomes turbulent, as seen for $\alpha = 7$ deg. As the angle of attack is increased, the location of the transition to turbulence moves upstream progressively until, for $\alpha > 12$ deg, the gage output rises abruptly at x/c = 0.02. The peak value increases until $\alpha = 13.5$ deg, when dynamic stall onset ensues. This event is seen clearly in Fig. 1c at the same x/c location and angle of attack. It is clear that the sharp rise corresponds to a dramatic increase in the local shear stress, and implies a singular flow event driving the local flow. It has been deduced from the earlier PDI studies (Ref. 1) that at M = 0.3, k = 0.05, dynamic stall onset occurs from the bursting of the laminar bubble and the present heat flux gage data clearly support that observation. It is intriguing to see such increasingly violent activity inside the bubble moving upstream when the angle of attack is increased, especially since the fluid contained in the bubble is deemed to be of low energy. Somehow, the fluid acquires the necessary energy to force itself upstream and cause an outburst from the leading edge of the bubble

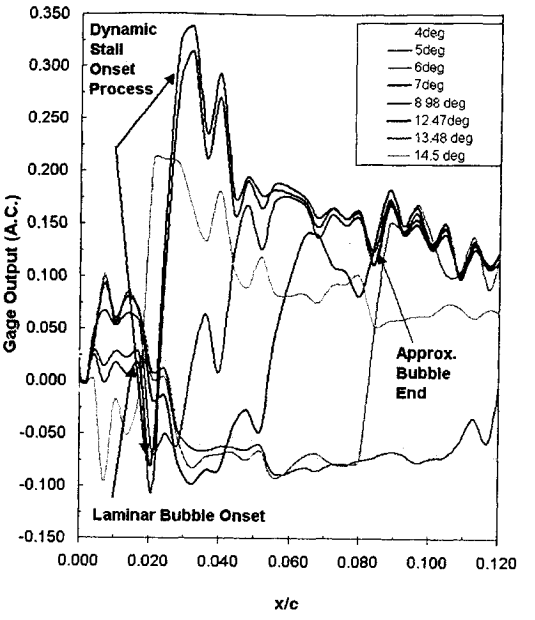

Fig. 2. Onset of Dynamic Stall from Bubble Bursting, M = 0.3, k = 0.05

that induces a bubble-bursting type of dynamic stall. In computational studies, Cui and Knight (Ref. 8) suggest a similar flow description. Subsequent to this event, the shear stress level falls ($\alpha = 14.5$ deg) as the vortex convects past the upper surface.

Figure 3 shows the details of the surface flow recorded using the sensors on the upper surface through the bubble region as the airfoil was pitched up for M = 0.3, k = 0.1. (In all the color images that follow, red represents the highest sensor output, blue the lowest, with green at the

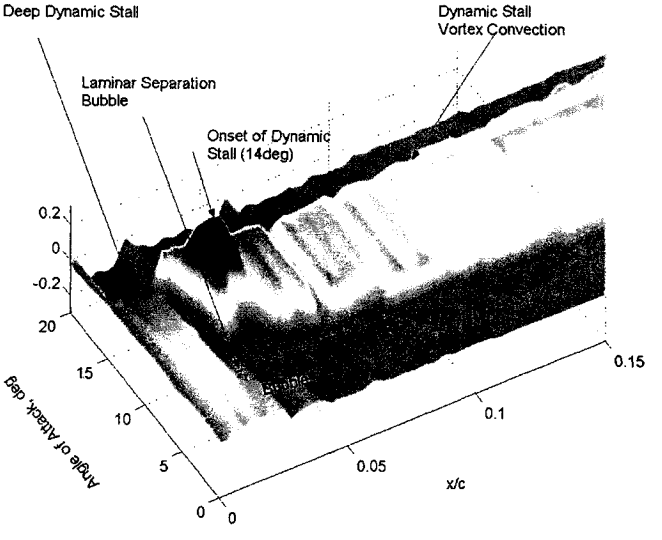

Fig. 3. Details of Flow in the Laminar Bubble, M = 0.3, k = 0.1

middle of the scale corresponding to the cycle mean value). These data are like those in Fig. 2 for M = 0.3, k = 0.05, except all traces are shown in the form of a continuous surface, whereas in Fig. 2 only eight traces were shown. The various features discussed above are also present for the higher reduced frequency and it is clear that dynamic stall arises from the leading edge of the bubble as it bursts. Another new result of value here is the fact that as the vortex grows and convects, the shear stress does not drop to zero or to a value where the fluid velocities are low (like in a typical dead-air region). The turbulence associated with the vortex and the flow on the backside of the vortex results in fairly large shear stress levels during its passage. At any location, the level falls off rapidly once the vortex passes.

Figures 4 and 5 compare the full upper surface flow fields for steady flow (obtained by slowly oscillating the airfoil at

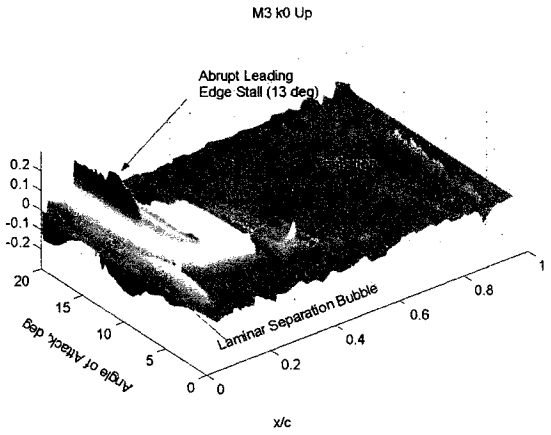

Fig. 4. Surface Shear Stress at M = 0.3, k = 0.001

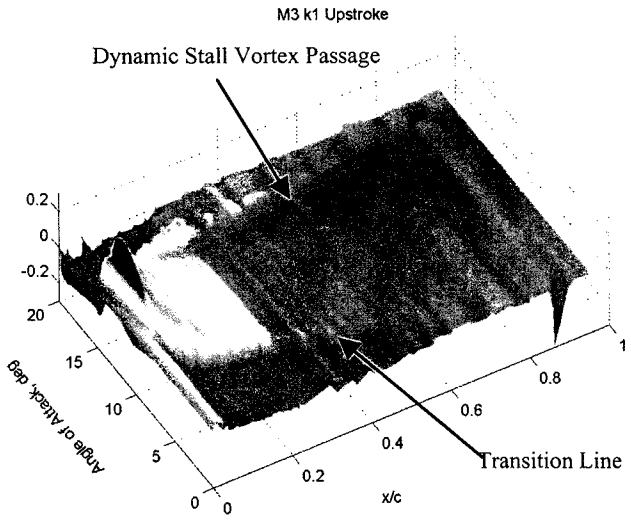

Fig. 5. Surface Shear Stress at M = 0.3, k = 0.1

k = 0.001, quasi-steady case) and k = 0.1 at M = 0.3. Fig. 4 shows that in steady flow, the airfoil experiences abrupt leading edge stall, which arises from the bubble bursting. Following this, the flow completely separates from the surface and extremely low shear stress values are seen. Even then, the unsteadiness in the shear layer can cause some intermittent reattachment just around the leading edge and hence, occasionally high values are seen locally past the static stall angle. On the other hand, Fig. 5 clearly shows the convection of the dynamic stall vortex for the unsteady case, k = 0.1 at M = 0.3. The vortex forms at $\alpha \approx$ 15 deg, moves over the airfoil, and is still seen on the surface for $\alpha \approx$ 17 deg. Prior to its arrival at a downstream location, the blue region over the surface in this figure suggests that a dead-air region is present.

C. Flow Details at M = 0.45, k = 0.05

Fig. 6 shows the PDI image at M = 0.45 for α = 6.9 deg. At this condition, the flow everywhere is subsonic and the only major flow feature is the laminar separation bubble that was typical in all cases. Many more fringes are seen in the image due to the higher Mach number. However, as the airfoil pitches up, for example by α = 9.5 deg, shocks form in the flow. These are a series of shock waves and expansion waves which have been explained as transonic flow interactions (Ref. 1). Fig. 7 shows a PDI image for this condition. The first shock is seen slightly ahead of the bubble origin and the others ride on top of the shear layer enveloping the bubble. Ref. 1 discusses the dynamic stall onset mechanism for this condition, which is primarily shock induced.

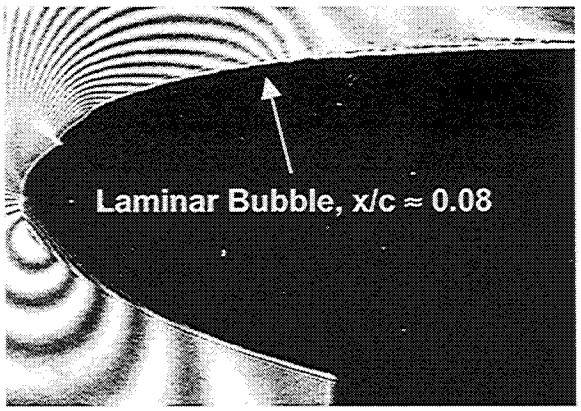

Fig. 6. PDI Image for M = 0.45, k = 0.05, $\alpha = 6.95^{\circ}$

The heat flux data for this flow condition at various angles of attack is shown in the lower half of Fig. 7. The bubble forms at a much earlier angle of attack of 5 deg, in comparison with M = 0.3 flow, and for α = 5 -7 deg, the bubble closes at x/c $\approx$ 0.08. At all angles shown, the activity in the bubble is low between x/c = 0.02 and x/c = 0.055. The distributions show slight waviness in the region ahead of the bubble onset location, but the trace for α = 9 deg shows a decrease and is then flat. The PDI studies showed a shock to first form at $\alpha \approx$ 9 deg. Since the static temperature rises across a shock wave, the heat transfer

from a heat flux gage at this location drops. Similarly, across an expansion wave, the heat transfer rises. The boundary layer near the leading edge where the shock forms is very thin (≈ 100 μm) and thus, the imprint of the shock can be picked up in the surface heat flux traces. However, the same cannot be seen within the bubble. Interestingly, as the angle of attack increases, the strength of the shock also increases and as shown in Fig. 7, its imprint becomes visible after the dynamic stall onset has begun. Here the gage output over x/c = 0.084 — 0.088 (which corresponds to one sensor) decreases sharply for several angles. On Fig. 7 is also shown the shock-induced dynamic stall onset point that is at x/c = 0.055. At this point, once again, the shear stress rises abruptly (over only one sensor). The gradients involved are very high, as discussed above, and are comparable to those seen for M°=°0.3. Beyond α = 12.5 deg, shock induced dynamic stall occurs. It is believed that dynamic stall origination in the middle of the bubble is due to the shock effects on the local recirculating flow region. In this flow, a weak shear layer envelops the bubble and on top of that rides a strong series of shocks. The events that normally occur inside the bubble for non-shock flow conditions appear to be accelerated and thus, dynamic stall occurs at a lower angle of attack at M = 0.45 compared to that at M = 0.3. Also, the origination mechanism of dynamic stall is due to these shocks as opposed to the natural bubble bursting.

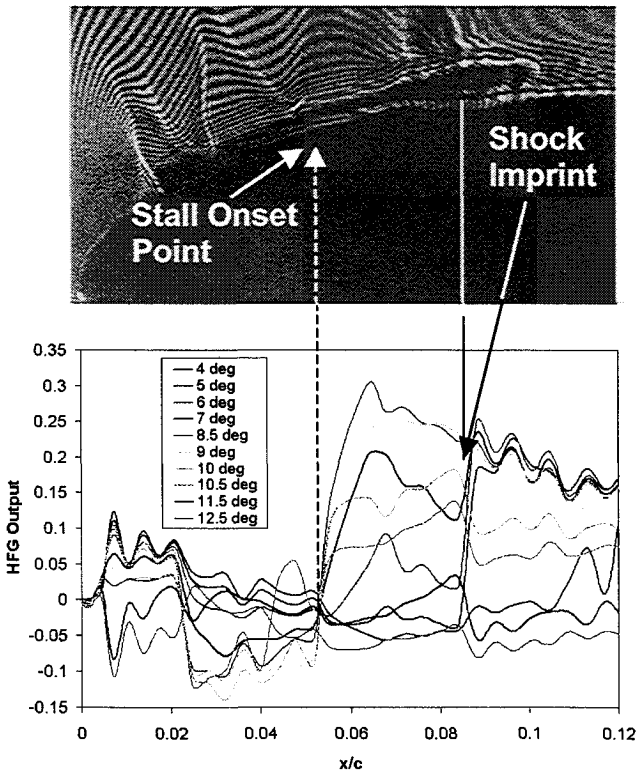

Fig. 7. Comparison of PDI at $\alpha = 9.5^{O}$ and Heat Flux Gage Data, M = 0.45, k = 0.05

D. Behavior of Transition

The compressible dynamic stall flow involves large changes in angle of attack and at model rotor Reynolds numbers (at which these tests were carried out), the airfoil boundary layer experiences transition and relaminarization during each cycle. Lack of the flow physics knowledge has been the primary limitation on proper computational modeling of this flow. This information can be generated from the data in hand since transition onset location can be determined accurately by using the rising heat flux values. Generally, the rise in heat flux due to transition is also preceded by gradually falling heat flux values due to the thickening of the laminar boundary layer. From the measurements obtained in this study it was possible to determine both the effect of Mach number and the effect of reduced frequency on transition behavior. These results provide the first recordings of the rapid upstream movement of the transition point in unsteady flow at these conditions.

Figure 8a shows the Mach number effect on transition movement at k = 0.05. It is seen that transition is accelerated when Mach number is increased (an effect partly due to the increasing Reynolds number associated with increasing the tunnel velocity at atmospheric conditions). Very low levels of heat flux result in a greater uncertainty in the effect beyond x/c = 0.7 (a < 0.5 deg). But, it is clear that transition starts near the trailing edge at very low angles of attack, (x/c = 0.6, α = 0.5 deg for M = 0.4, or x/c = 0.6, α ≈ 1 deg for M = 0.3) and moves rapidly upstream. The behavior becomes increasingly nonlinear (see the polynomial curve fit to the data) as the angle of attack increases, with an x/c movement of nearly 0.1 from α = 3-4 deg for M = 0.4. Once the laminar bubble forms,

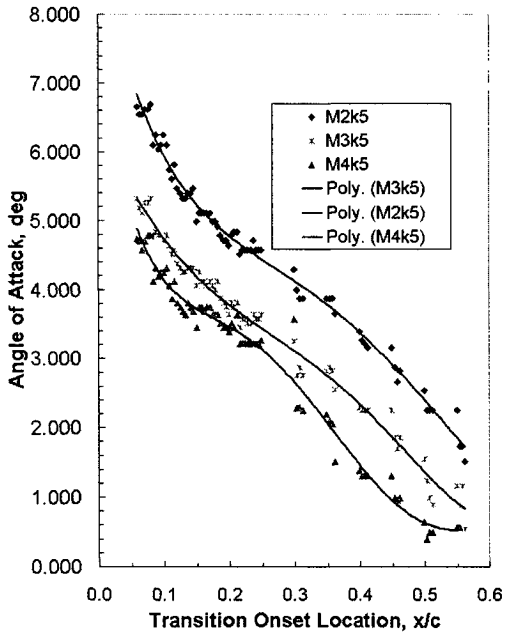

Fig. 8a. Effect of Mach Number on Transition Behavior, k = 0.05

the upstream progression is even more rapid.

Figure 8b shows the effect of reduced frequency at M = 0.3. It is interesting to see that transition onset is progressively delayed by increasing the degree of unsteadiness (k), with the same nonlinear behavior prevailing. Like for the previous case, the movement becomes more rapid as the angle of attack exceeds 3-4 deg.

Most dynamic stall computations have hitherto been either fully turbulent or fully laminar, with very few exceptions (for example, Ref. 9). Even in Ref. 9, the transition onset has been fixed for the most part to be very near the suction peak location. It is critical to include this information in the modeling, as well as the fact that the reattaching boundary layer relaminarizes, as will be shown in the next section, for any appropriate flow physics to be modeled through CFD analysis.

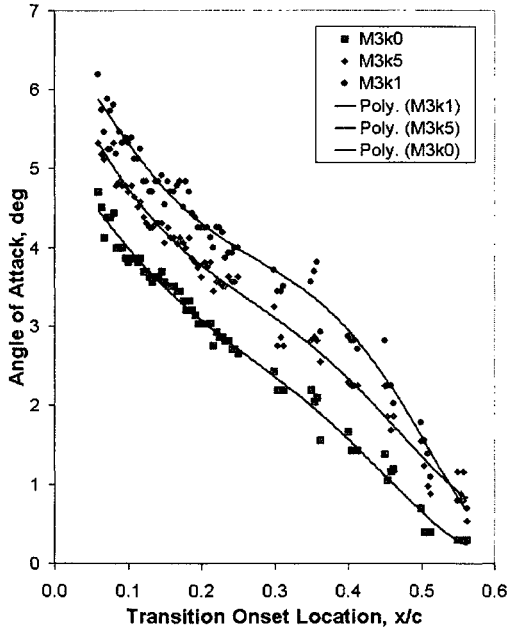

Fig. 8b. Effect of Reduced Frequency on Transition Behavior, M = 0.3

E. Reattachment of Dynamic Stall Flow

Figures 9a and 9b show the reattachment of the deep dynamic stall flow on the downstroke for two cases. Fig. 9a shows the results for the conditions of M = 0.2, k = 0.1. The separated shear layer is highly turbulent and unsteady, but its surface imprint is basically void in heat transfer. The void in the heat flux remains for much of the deep stall phase until the airfoil is at around 12 deg on the downstroke when the flow begins to reattach. This process starts from the leading edge as a turbulent process and proceeds in a systematic way as indicated in Fig. 9a. When the airfoil angle of attack has decreased substantially, the boundary layer near the leading edge begins to relaminarize first as the process continues. Eventually, at very low angles of attack ≈ 1 deg the entire flow becomes laminar, as seen in Fig. 9a. A laminar bubble also forms during this process (see Ref. 10) as shown in the figure.

Similarly, for M = 0.45, k = 0.05, the deep stall flow has very little surface shear stress (blue regions in the figure), but around α = 10 deg, the shear layer begins to reattach. The higher Reynolds number of the flow results in higher local shear stress during reattachment and relaminarization takes place in this case at even lower angles. It thus seems that even though the dynamic stall onset mechanism for the higher Mach number case is different, the reattachment process is largely similar, with only some differences in the angles at which the various events occur.

These details provide a clear documentation of the large changes in the transition and the surface shear stress that occur in this complex flow, a fact that needs to be included in the CFD modeling of the flow. Considerably better agreement with experimental data can be obtained if the appropriate physics such as described above are included in the models.

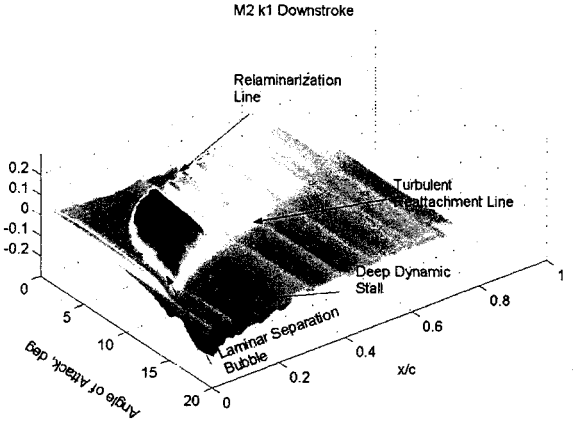

Fig. 9a. Reattachment of Dynamic Stall Flow, M = 0.2, k = 0.1

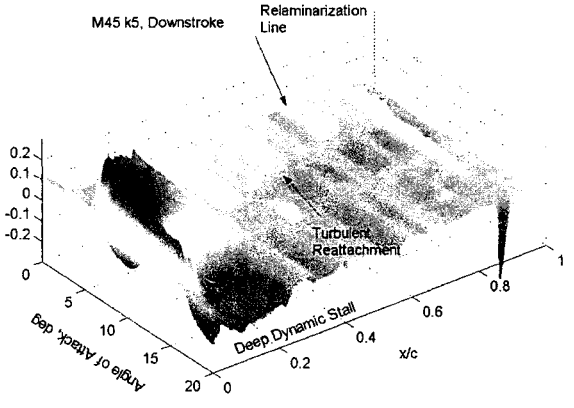

Fig. 9b. Reattachment of Dynamic Stall Flow, M = 0.45, k = 0.05

4. Concluding Remarks

The study has revealed the various surface flow features of compressible dynamic stall and their changes under different flow conditions. It has also provided a description of the events that are precursors to dynamic stall onset. The imprint of a leading edge shock has been recorded for the first time in the surface flow signature.

The dominant features of the flow are:

a) the rapid movement of the transition point in the unsteady flow over the airfoil, that can now be included in the computational modeling of the flow
b) the formation of the dynamic stall vortex from
   i. the leading edge of the bursting of the laminar separation bubble, and
   ii. at higher Mach numbers, shock induced flow separation from somewhere in the middle of the bubble.

In all cases of stall observed, there is an extremely rapid rise of the surface shear stress. This is believed to be the first experimental documentation of such flow physics in these complex flows. The data indicate that extremely large gradients develop prior to onset of dynamic stall, pointing to a singular event that drives the flow into the stalled state. Since this rapid rise in the shear stress has been seen to be a precursor to dynamic stall for different flow conditions and widely different dynamic stall onset mechanisms, it is believed that similar flow physics will also prevail in full scale rotor dynamic stall. A definitive result can be obtained by repeating the present studies on a tripped airfoil.

Acknowledgements

This work was supported by Army Research Office under grant no. MIPR0KNPGAS052 to the US Naval Postgraduate School and monitored by T.L.Doligalski. The heat flux gage sensors on the airfoil were installed at NASA Langley Research Center with design help from J.L.Bartlett. The discussions with L.W.Carr, S.S.Davis and the support of the NASA Ames Fluid Mechanics Laboratory staff are gratefully acknowledged.

5. References

1. M.S.Chandrasekhara, M.C.Wilder, L.W.Carr, Competing Mechanisms of Compressible Dynamic Stall, *AIAA Journal*, Vol. 36, No. 3, 1998, pp. 387-393.
2. J.W.Kiedaisch, M.Acharya, Investigation of Incipient Dynamic Stall Over Pitching Airfoils Using Hot-Film Sensors, AIAA 97-0656, 35th Aerospace Sciences Meeting and Exhibit, Jan. 6-10, 1997, Reno, NV.
3. T.Lee, S.Basu, Measurement of Unsteady Boundary Layer Developed on an Oscillating Airfoil Using Multiple Hot-Film Sensors, *Experiments in Fluids*, Vol. 25, No. 1, 1998, pp. 108-117.
4. S.J.Schreck, W.E.Faller, H.E.Helin Pitch Rate and Reynolds Number Effects on Unsteady Boundary Layer Transition and Separation, *AIAA Journal of Aircraft*, Vol. 35, No. 1, 1998, pp. 46-52.
5. S.J.Schreck, W.E.Faller, M.C.Robinson, Unsteady Separation Processes and Leading Edge Vortex Precursors: Pitch Rate and Reynolds Number Influences, AIAA 2000-2605, Fluids 2000 Conference, Jun. 19-22, 2000, Denver, CO.
6. A.Nakayama, J.P.Stack, J.C.Lin, W.O.Valarezo, Surface Hot-Film Technique for Measurements of Transition, Separation, and Reattachment Points, AIAA 93-2918, 24th Fluid Dynamics Conference, Jul. 6-9, 1993, Orlando, FL.
7. J.P.Stack, S.M.Mangalam, S.A.Berry, A Unique Measurement Technique to Study Laminar-Separation Bubble Characteristics on an Airfoil, AIAA 87-1271, 19th Fluid Dynamics, Plasma Dynamics and Lasers Conference, Jun. 8-10, 1987, Honolulu, HI.
8. Cui and D.D.Knight, Parallel Computation of the 2-D Navier-Stokes Flowfield of a Pitching Airfoil, *Computational Fluid Dynamics*, 1995, Vol. 4, pp. 111-135.
9. W.Geissler, L.W.Carr, M.S.Chandrasekhara, M.C.Wilder and H.Sobieczky, Compressible Dynamic Stall Calculations Incorporating Transition Modeling for Variable Geometry Airfoils, AIAA Paper 98-0705, Reno, NV, Jan. 1998.
10. S.Ahmed, and M.S.Chandrasekhara, Reattachment Studies of an Oscillating Airfoil Dynamic Stall Flow Field, (AIAA Paper 91-3225), *AIAA Journal*, Vol. 32, No. 5, May 1994, pp. 1006 - 1012.